Redox Biology 28 (2020) 101337

Contents lists available at ScienceDirect

Redox Biology

journal homepage: www.elsevier.com/locate/redox

AMPK-mediated senolytic and senostatic activity of quercetin surface functionalized Fe_3O_4 nanoparticles during oxidant-induced senescence in human fibroblasts

Anna Lewinska[a,1], Jagoda Adamczyk-Grochala[a,1], Dominika Bloniarz[b], Jakub Olszowka[c], Magdalena Kulpa-Greszta[d], Grzegorz Litwinienko[e], Anna Tomaszewska[f], Maciej Wnuk[c,*], Robert Pazik[f,**]

[a] Department of Cell Biochemistry, Faculty of Biotechnology, University of Rzeszow, Pigonia 1, 35-310, Rzeszow, Poland
[b] Department of Perinatology, Institute of Midwifery and Medical Emergency, Faculty of Medicine, University of Rzeszow, Pigonia 6, 35-310, Rzeszow, Poland
[c] Department of Genetics, Faculty of Biotechnology, University of Rzeszow, Pigonia 1, 35-310, Rzeszow, Poland
[d] Faculty of Chemistry, Rzeszow University of Technology, Powstancow Warszawy 12, 35-959, Rzeszow, Poland
[e] Faculty of Chemistry, University of Warsaw, Pasteura 1, 02-093, Warsaw, Poland
[f] Department of Medicinal Chemistry and Nanomaterials, Faculty of Biotechnology, University of Rzeszow, Pigonia 1, 35-310, Rzeszow, Poland

ARTICLE INFO

Keywords:
Quercetin surface functionalized Fe_3O_4 nanoparticles
Hydrogen peroxide
Senescence
Senolytics
Senostatics
Fibroblasts

ABSTRACT

Cellular senescence may contribute to aging and age-related diseases and senolytic drugs that selectively kill senescent cells may delay aging and promote healthspan. More recently, several categories of senolytics have been established, namely HSP90 inhibitors, Bcl-2 family inhibitors and natural compounds such as quercetin and fisetin. However, senolytic and senostatic potential of nanoparticles and surface-modified nanoparticles has never been addressed. In the present study, quercetin surface functionalized Fe_3O_4 nanoparticles (MNPQ) were synthesized and their senolytic and senostatic activity was evaluated during oxidative stress-induced senescence in human fibroblasts *in vitro*. MNPQ promoted AMPK activity that was accompanied by non-apoptotic cell death and decreased number of stress-induced senescent cells (senolytic action) and the suppression of senescence-associated proinflammatory response (decreased levels of secreted IL-8 and IFN-β, senostatic action). In summary, we have shown for the first time that MNPQ may be considered as promising candidates for senolytic- and senostatic-based anti-aging therapies.

1. Introduction

Cellular senescence, a state of permanent cell cycle arrest and increased secretion of proinflammatory factors, is a complex phenomenon that may contribute to different biological outcomes such as tumor suppression, tumor promotion, aging and tissue repair [1–3]. Thus, senescent cells may promote both beneficial effects by proinflammatory response-mediated recruitment of immune cells to eliminate damaged cells and stimulation of proliferation and differentiation of neighbouring cells (tissue remodeling) and protection against propagation of damaged dysfunctional precancerous cells (inhibition of tumorigenesis) and detrimental effects by chronic inflammation (induction of tumorigenesis and aging) [1–3]. Senescent cells accumulate in the body over time. However, the underlying molecular mechanism is largely unknown. More recently, it has been documented that senescent dermal fibroblasts may escape from immune clearance by the non-classical MHC molecule HLA-E-mediated inhibition of the inhibitory receptor NKG2A-expressing NK and $CD8^+$ T cells and blocking the interaction between HLA-E and NKG2A by RNAi-based inhibition of HLA-E expression stimulates the immune response against senescent cells *in vitro* [4]. As cellular senescence may be a driver of aging and age-related diseases, one can suggest that the removal of senescent cells from tissues and organs might be clinically important [5,6]. To do so, transgenic and pharmacological approaches have been already considered, namely the construction of genetic animal models and search for small molecules that may specifically kill senescent cells (termed senolytics)

* Corresponding author.
** Corresponding author.
E-mail addresses: mwnuk@ur.edu.pl (M. Wnuk), rpazik@ur.edu.pl (R. Pazik).
[1] These authors have contributed equally as first authors.

https://doi.org/10.1016/j.redox.2019.101337
Received 29 August 2019; Received in revised form 22 September 2019; Accepted 1 October 2019
Available online 04 October 2019

[7–17]. Thanks to a well established biomarker of senescence, $p16^{Ink4a}$, a cyclin-dependent kinase inhibitor, that is transcriptionally active in senescent cells and the use of INK-ATTAC (INK-linked apoptosis through targeted activation of caspase, a transgenic suicide gene) strategy, it has been documented that the induction of apoptosis in $p16^{Ink4a}$-expressing cells of BubR1 progeroid mice limited the progeroid phenotype [7]. Moreover, in wild-type mice, the clearance of senescent cells extended median lifespan, delayed tumorigenesis and attenuated age-related changes in several tissues [8]. Senolytic action of targeted therapeutics, e.g., a non-specific tyrosine kinase inhibitor dasatinib, inhibitors of Bcl-2 family of antiapoptotic proteins, HSP90 inhibitors, and a modified FOXO4-p53 interfering peptide as well as plant-derived natural substances, e.g., quercetin, fisetin, piperlongumine and curcumin analog EF24 has been also reported [10-16,18-21]. Quercetin (3,3',4'5,7-pentahydroxyflavone) is a natural flavonol found abundantly in vegetables and fruits [22–24]. Antioxidant, anti-inflammatory and anti-cancer activity of quercetin is well established in numerous cellular and animals models as well as in humans [22–24]. Thus, several therapeutic applications of quercetin have been suggested, namely for prevention and treatment of e.g., cancer, cardiovascular and neurodegenerative diseases [22–24]. At molecular level, quercetin-mediated action is based on modulation of signaling pathways and gene expression, and cellular targets of quercetin may be transcription factors, cell cycle proteins, pro- and anti-apoptotic proteins, growth factors and protein kinases, e.g., NF-κB, cyclin D1, Bax, Bcl-2, caspase, PARP and Gadd 45 [25].

In general, senolytic-mediated elimination of senescent cells may be cell-type specific [16]. For example, dasatinib killed senescent human fat cell progenitors, quercetin was more active against senescent human umbilical vein endothelial cells (HUVECs) and mouse bone marrow-derived mesenchymal stem cells (BM-MSCs) and the combination of dasatinib and quercetin eliminated senescent mouse embryonic fibroblasts (MEFs) [10]. The use of natural polyphenols as senotherapeutics may be limited due to their poor water solubility, chemical instability and low bioavailability, however, this may be partially overcome by the applications of selected delivery systems, namely lipid-based carriers, polymer nanoparticles, inclusion complexes, micelles and conjugates-based delivery systems [26]. Moreover, senescent cells with elevated activity of lysosomal β-galactosidase can be targeted and selectively killed by the use of cytotoxic agents encapsulated with β(1,4)-galacto-oligosaccharides [27].

As there is no information on nanoparticle-mediated senolytic action in biological systems, we have decided to synthesize magnetite nanoparticles and modify their surface using quercetin-based coating, and evaluate the senolytic activity of quercetin surface functionalized magnetite nanoparticles (MNPQ) using the model of hydrogen peroxide-induced premature senescence and human fibroblasts as a well established system to study cellular senescence *in vitro* [28]. Moreover, the ability of MNPQ to attenuate senescence-associated proinflammatory responses, namely based on interleukin 8 (IL-8) and interferon beta (IFN-β) (termed senostatic activity) [29] was also assayed. MNPQ treatment during stress-induced premature senescence (SIPS) resulted in elimination of senescent cells and limited secretion of IL-8 and IFN-β that was accompanied by elevated activity of AMP-activated protein kinase (AMPK).

2. Materials and methods

2.1. Synthesis of Fe_3O_4 nanoparticles

For the fabrication of the Fe_3O_4 nanoparticles, a well known synthetic strategy has been chosen and described in detail elsewhere [30]. In order to prepare the Fe_3O_4 nanoparticles, 2.1192 g (6 mmol) of Fe $(acac)_3$ (99.99%, Alfa Aesar, Warsaw, Poland) were dissolved in 70 ml of acetophenone (99%, Sigma Aldrich, Poznan, Poland; used without further purification) resulting in an intense red solution at room temperature. The prepared mixture was thermally decomposed under reflux for 4 h. After that black suspension containing Fe_3O_4 nanoparticles was obtained. The final product was separated by fast centrifugation, washed with 20 ml of ethanol (96%, POCh, Gliwice, Poland) six times for acetophenone removal and re-suspended in ethanol stock solution. The concentration of resulting nanoparticle suspension was determined as 9 mg/ml.

2.2. Surface modification

Since the quercetin solubility is extremely limited in water, surface functionalization of the Fe_3O_4 nanoparticles was performed by addition of 300 mg quercetin into the 3 ml of Fe_3O_4 ethanol dispersion containing 27 mg of magnetite nanoparticles. The end-volume of the mixture was set to 15 ml by addition of ethanol. Afterwards cap protected test-tube containing mixture of nanoparticles and quercetin was placed into ultrasonic bath for 60 min and sonicated at 40 °C. The quercetin grafted magnetite dispersion was further purified by centrifugation and washing with ethanol in order to remove not anchored ligand which has been added with great extent. The purification step was repeated four times. Afterwards surface functionalized Fe_3O_4 magnetite particles were re-suspended in an ultra pure water, transferred into brown glass vial and stored in a laboratory fridge at 5 °C for prolonged durability of stock MNPQ colloidal suspension. The final concentration of quercetin modified Fe_3O_4 nanoparticles was adjusted to 1 mg/ml and used for further characterization.

2.3. Characterization of nanoparticles

Structural properties of the materials were verified by means of X-ray powder diffraction (XRD) measurements by using Bruker D8 Advance diffractometer equipped with the Cu lamp ($K\alpha_1$: 1.54060 Å) and Ni filter. Primary particle size, morphology and selective area electron diffraction were elaborated using transmission electron microscopy (TEM) with Tecnai Osiris X-FEG HRTEM microscope operating at 200 kV. For TEM characterization, a droplet of ethanol nanoparticle dispersion (0.25 mg/ml) was placed on a carbon covered copper microscope grid and left overnight until complete sample drying. Particle diameter was determined using volume-weighted equation:

$$d_{av} = \sum \frac{n_i d_i^4}{n_i d_i^3}, \quad (1)$$

where d_{av} is defined as the mean primary size of particles, n_i is the number of particles of given size and d_i is a diameter of i particle. The concentration of nanoparticles in the final suspension was estimated by microscaling technique using Radwag MYA 5.4Y balance by placing 50 µl of stock dispersion on aluminium crucible and evaporating the solvent to a dry mass. The procedure was repeated three times.

Hydrodynamic size of nanoparticle suspensions was measured using dynamic light scattering technique (DLS), whereas zeta potential was determined by means of electrophoretic light scattering (ELS) utilizing universal Nanoplus HD 3 system from Particulate System/Micrometrics equipped with 660 nm laser diode and autotitrator. The size analysis of particles was done using dedicated software provided by the manufacturer of equipment. Prior hydrodynamic size and zeta potential characterization, water based stock suspensions of Fe_3O_4 nanoparticles and quercetin modified Fe_3O_4 nanoparticles of a concentration of 1 mg/ml were prepared and further diluted. In the case of zeta potential, dilution of nanoparticles and dispersions of quercetin grafted nanoparticles were prepared using 0.001 M KCl electrolyte to prevent from non-homogeneous distribution of the electric field. Usually working concentrations assuring repeatable measurements of both nanoparticle dispersions were between 60 µg/ml or 30 µg/ml. In order to give a direct evidence of successful surface functionalization with quercetin, Fourier transform infrared spectra were recorded with a Thermo

Scientific Nicolet iZ10 FT-IR spectrometer equipped with Smart Orbit Diamond ATR (attenuated total reflection) accessory in the range of 4000-500 cm^{-1}at room temperature. Dried suspensions of Fe_3O_4 pure nanoparticles together with quercetin anchored Fe_3O_4 nanoparticles were gently grinded in an agate mortar and directly placed on the diamond surface of ATR accessory. As a reference standard, pure quercetin and bare nanoparticles were used without any specific treatment. Thermogravimetric (TGA) measurements were performed with TA Instruments Q50 V20.13 thermogravimetric analyzer (precision ± 0.01%, sensitivity 0.1 μg) employing platinum vessels. Two-points temperature calibration was performed. Tests with decomposition of standard material (calcium oxalate monohydrate) were successful. The samples were heated under nitrogen flow (6 dm^3/h), at a rate of 5 °C/min from 25 up to 1000 °C. All TG measurements were analyzed by means of Universal V4.5° program in order to determine mass change and the temperature of decomposition.

2.4. Cell culture

Human foreskin fibroblasts BJ (maximum population doubling level, PDL = 72, ATCC® CRL-2522™) were obtained from American Type Culture Collection (ATCC, Manassas, VA, USA) at PDL 24. BJ cells at PDLs between 26 and 40 (10000 cells/cm^2) were cultured at 37 °C in Dulbecco's Modified Eagle's medium (DMEM) containing 10% fetal calf serum (FCS), 100 U/ml penicillin, 0.1 mg/ml streptomycin and 0.25 μg/ml amphotericin B (Sigma-Aldrich, Poznan, Poland) in a cell culture incubator in the presence of 5% CO_2. BJ cells were passaged using trypsin-EDTA solution (Sigma-Aldrich, Poznan, Poland) and PDL was calculated as previously described [31]. To induce oxidant-mediated senescence, BJ cells were treated with 100 μM hydrogen peroxide for 2 h [31] and then cells were stimulated with quercetin (Q), unmodified Fe_3O_4 nanoparticles (MNP) and quercetin surface functionalized Fe_3O_4 nanoparticles (MNPQ) at the concentration of 5 μg/ml for 24 h. The solvent used (here ethanol) had no effect on cell viability. For a 7-days experiment, cells were also treated with hydrogen peroxide (100 μM) for 2 h and with Q, MNP and MNPQ (5 μg/ml) for 24 h, but then Q, MNP and MNPQ were removed and cells were cultured in Q-, MNP- and MNPQ-free DMEM medium for up to 7 days. Every 48 h, the cell culture medium was replaced by a fresh one.

2.5. Selection of non-cytotoxic MNPQ concentration

To study the senostatic and senolytic activity of MNPQ during hydrogen peroxide-induced senescence in BJ cells, non-cytotoxic concentration of MNPQ (5 μg/ml) was selected on the basis of MTT test and the analysis of reactive oxygen species (ROS) levels. Briefly, BJ cells were seeded onto a 96-well plate at the concentration of 5000 cells per a well and after 24 h of culture, Q, MNP and MNPQ were added at the concentrations ranging from 2.5 to 15 μg/ml for additional 24 h and metabolic activity was then analyzed [32]. Moreover, Q-, MNP- and MNPQ-mediated oxidative stress was analyzed using Muse™ Cell Analyzer and Muse™ Oxidative Stress Kit (Merck Millipore, Warsaw, Poland) as described comprehensively elsewhere [33]. The concentration of 5 μg/ml that did not induce significant changes in metabolic activity and intracellular redox homeostasis was selected for further analysis.

2.6. Cell proliferation and cell cycle

The cell number was automatically calculated using TC10™ Automated Cell Counter (Bio-Rad, Hercules, CA, USA). Moreover, a marker of cell proliferation was considered, namely Ki67. The subpopulations of Ki67-positive and Ki67-negative cells were revealed using Muse™ Cell Analyzer and Muse™ Ki67 Proliferation Kit (Merck Millipore, Warsaw, Poland). DNA-based cell cycle analysis was performed using Muse™ Cell Analyzer and Muse™ Cell Cycle Kit according to the manufacturer's instructions (Merck Millipore, Warsaw, Poland) [31].

2.7. Cell death

Apoptosis was assayed using Muse™ Cell Analyzer and Muse™ Annexin V and Dead Cell Assay Kit (Merck Millipore, Warsaw, Poland) as previously described [32]. Moreover, to reveal necrotic mode of death, trypan blue dye exclusion assay was considered. Briefly, cells were incubated with 0.4% trypan blue and then dead cells with porous cell membranes (blue-stained cells) were automatically scored using TC10™ Automated Cell Counter (Bio-Rad, Hercules, CA, USA).

2.8. Senescence-associated β-galactosidase activity (SA-β-gal)

BJ cells were treated with 100 μM hydrogen peroxide for 2 h to promote stress-induced premature senescence (SIPS) [31] and then treated with 5 μg/ml Q, MNP and MNPQ for 24 h, and 7 days after removal of Q, MNP and MNPQ, SA-β-gal activity was analyzed as previously reported [33].

2.9. Imaging flow cytometry

BJ cells (10^6 cells) were fixed using 4% solution of *p*-formaldehyde in PBS containing 0.01% Triton X-100 at room temperature for 10 min, washed using PBS and suspended in 70% ethanol at 4 °C for 20 min. To avoid unspecific binding, fixed cells were pre-incubated with 1% BSA in PBS for 20 min and then incubated with primary antibodies anti-p53 (1:200, MA5-12557) and anti-p21 (1:200, MA5-14949) at room temperature for 1 h and secondary antibody conjugated to Alexa Fluor Plus 488 (1:1000, A32723, A32731) (Thermo Fisher Scientific, Warsaw, Poland) at room temperature for 1 h. Fixed cells were then stained using 5 μg/ml PI solution for 10 min. Digital cell images were captured and intracellular localization of p21 and p53 was analyzed using flow imaging cytometry (Amnis® FlowSight® imaging flow cytometer and IDEAS software version 6.2.187.0, Merck Millipore, Warsaw, Poland).

2.10. Western blotting

Protein extraction and Western blotting protocol was applied as previously described [34]. For evaluation of LC3BII levels, cells were also stimulated with 50 μg/ml chloroquine for 6 h. The following primary and secondary antibodies were used: anti-IL8 (1:200, ab154390), anti-IFN-β (1:200, ab176343), anti-AMPKα (1:1000, 5832), anti-phospho-AMPKα (Thr172) (1:1000, 2535), anti-AKT (1:1000, 4691), anti-phospho-AKT (Ser473) (1:1000, 4060), anti-LC3B (1:750, 2775), anti-GLUT1 (1:1000, PA1-46152), anti-p21 (1:1000, MA5-14949), anti-p53 (1:1000, MA5-12557), and HRP-linked antibodies anti-β-actin (1:40000, A3854), anti-rabbit IgG (1:3000 or 1:1000, 7074) and anti-mouse IgG (1:3000, 7076) (Thermo Fisher Scientific, Sigma-Aldrich, Abcam and Cell Signaling Technology). The data represent the relative density normalized to β-actin. Phospho-AMPKα and phospho-AKT signals were also normalized to AMPKα and AKT signals, respectively. The levels of IL8 and IFN-β in post-culture supernatants were calculated per 10^4 cells.

2.11. Extracellular acidification rate (ECAR) and oxygen consumption rate (OCR)

MNPQ-mediated changes in extracellular acidification rate (ECAR) and oxygen consumption rate (OCR) in BJ cells were assayed using Seahorse XFp Analyzer (Seahorse Bioscience, Billerica, USA) based on a 8-well miniplate format. Briefly, cells were seeded at a density of 1×10^4 cells per well and cultured overnight. Then, cells were treated with 100 μM hydrogen peroxide for 2 h and then with Q, MNP or MNPQ (5 μg/ml) for 24 h prior to the measurement. For ECAR analysis, glucose, oligomycin and 2-deoxy-D-glucose (2-DG) were used according to

the manufacturer's instructions (Glycolysis Stress Test, 103020-100, Agilent, California, USA). For OCR analysis, oligomycin, carbonyl cyanide 4-(trifluoromethoxy) phenylhydrazone (FCCP), rotenone and antimycin A were used according to the manufacturer's instructions (Cell Mito Stress Test, 103015-100, Agilent, California, USA).

2.12. Statistical analysis

The results represent the mean ± SD from at least three independent experiments. Statistical significance was assessed by 1-way ANOVA using GraphPad Prism 5, and with the Dunnett's multiple comparison test.

3. Results

3.1. Characterization of magnetite nanoparticles and quercetin grafted nanoparticles

Crystal structure of the Fe_3O_4 nanoparticles was confirmed by the X-ray powder diffraction technique on the basis of direct comparison of recorded pattern with the reference card number 19–0629 from the ICSD database (Fig. 1A).

All the Bragg's reflections correspond well with the cubic Fe_3O_4 and no other peaks were detected confirming structural purity of the final product (Fig. 1A). Significant noise levels on the X-ray diffraction pattern are due to the high ferrite matrix X-ray absorption (Fig. 1A).

The particles diameter was evaluated using three distinctly different methods: calculation based on a well known Scherrer's equation [35] allowing for rough but quick and easy estimation of the crystallite size directly from the diffraction peaks, transmission electron microscopy of the dried powders - so called primary size of particles which gives the realistic particle size and lastly more adequate, in view of biological implementation of the given material, DLS technique for the study of objects diameter (single particles, agglomerates etc.) present in a liquid media (here water based). The average crystallite size was calculated using following formula:

$$D = \frac{k\lambda}{\cos\sqrt{\beta^2 - \beta_0^2}}, \quad (2)$$

where D stands for the grain size; β_0 –apparatus broadening; β – full width at half maximum; Θ- angle; k constant (usually equal to 0.9), and λ is an X-ray wavelength gives the value of 12 nm, which is rather close to that obtained from the analysis of TEM images of particles (14 nm). This value is fairly consistent with our previous report devoted to the synthetic issues in preparation of the MFe_2O_4 family [36]. The hydrodynamic size has been measured for both pure Fe_3O_4 and quercetin grafted Fe_3O_4 nanoparticles dispersions in water (Fig. 1B). It is quite obvious that the state of the particle water suspensions is of great importance in biological applications. Therefore, it is necessary to monitor the hydrodynamic particle size, its distribution and zeta potential (defining the colloidal stability and highly prone to even small changes done on the dispersion). In case of the bare Fe_3O_4 nanoparticles, the hydrodynamic diameter was estimated to be around 140 nm (PdI polydispersity index – 0.11) (Fig. 1B) pointing out on the presence of loosely agglomerated particles. This is actually not a surprise since the material has not been covered with any kind of surfactant or protecting ligand. Moreover, this behavior finds its reflection in the TEM imaging as well (Fig. 1C). One can easily identify presence of particle agglomerates. Grafting of the fairly large quercetin molecules led to the formation of bigger particle clusters with size around 1.2 μm (PdI – 0.33) (Fig. 1B) which might be caused by rather low hydrophilic character of the quercetin (extremely low solubility in water). It is also important to note that the zeta potential of the dispersion containing pure Fe_3O_4 particles was around 23 mV whereas addition of quercetin leads to lower zeta potential value of 10 mV. Thus, the colloidal stability of Fe_3O_4 nanoparticles with anchored quercetin ligand is remarkably lower than without it (in both cases the pH of the final dispersions was close to neutral).

The FTIR-ATR absorption spectra were recorded in order to get a more detailed insight into effectiveness of quercetin ligand grafting on the surface of the Fe_3O_4 nanoparticles (Fig. 1D). As a reference samples, pure quercetin and Fe_3O_4 particles were measured and directly compared with Fe_3O_4 sample functionalized with quercetin (Fig. 1D). The IR spectra of pure quercetin consists of a very characteristic vibrational bands at positions accurately corresponding with previous reports (Fig. 1D) [37–40]. The most prominent are: OH band assigned to the phenolic hydroxyl bonding (stretching) at 3386 cm^{-1}, C═O carbonyl functional group (aryl ketonic stretch) at 1666 cm^{-1}, OH bending associated with the phenol function at 1351 cm^{-1}, group of vibrations corresponding to the stretching of aryl ether ring C–O at 1236 cm^{-1}, phenol C–O at 1207 cm^{-1} and in ketone C–CO–C 1160 cm^{-1}, respectively (Fig. 1D). Furthermore, characteristic vibrations of the aromatic ring C═C at 1610, 1560 and 1510 cm^{-1}, in-plane bending of C–H in aromatic hydrocarbon at 1317 cm-1, as well as several out of plane bands at 933, 817, 699 and 600 cm^{-1} were revealed (Fig. 1D). In the case of pure Fe_3O_4 nanoparticles, one can distinguish a broad band located at around 560 cm^{-1} due to the vibration of the Fe–O bonds as well as at around 3380 cm^{-1} due to the water content (after particle separation and drying from water based dispersion) (Fig. 1D). One can find also several very broad and hard to allocate vibrations within 1000 - 1600 cm^{-1} spectral range which nature probably can be attributed to the presence of some residual organic left after the preparation process (Fig. 1D). This can be associated with the mechanism of particle formation described in a great detail by Kessler et. al. [41,42]. Upon comparison with the quercetin grafted Fe_3O_4 sample, it can be noted that, almost all above discussed peaks were observed as well. However, the main difference relies in their decreased intensity. Several bands attributed to the quercetin ligand were also down-shifted (Fig. 1D). Most affected were those ascribed to the C═O of aryl ketone functional group, C–O and OH vibrations at phenyl part and C═C, respectively pointing out on interactions between the ferrite inorganic matrix and the quercetin causing slight variations in bond lengths (Fig. 1D). It is worth noting that vibrations associated with the OH groups are broadened which could suggest formation of hydrogen bonds between hydroxyl groups present at the surface of the Fe_3O_4 (Fig. 1D). This behavior gives a direct evidence of successful functionalization of the Fe_3O_4 nanoparticle surface with quercetin.

Thermo-gravimetric analysis of quercetin grafted Fe_3O_4 nanoparticles was conducted under nitrogen atmosphere up to 1000 °C in order to estimate the amount of quercetin attached to the particles surface (Fig. 1E). Thermal behavior of the reference quercetin follows typical decomposition stages of the thermally stable organic compounds, with a fast decomposition step (47.5% of mass loss) within the range 250–375 °C, followed by a two-step slow decomposition (ca. 31% at 400–800 °C, and 15% at 800–1000 °C range) with 6.5% of residue after the experiment is finished. The pure Fe_3O_4 nanoparticles show generally a mass reduction attributed to the loss of physisorbed water/ethanol mixture below 200 °C (around 2.2%) and further pyrolysis of small amount of residual organics (remains after synthesis) until stabilization of the sample mass (Fig. 1E). TG curve recorded for magnetite coated with quercetin exhibit good thermal stability below 250 °C followed by rapid weight loss at range 250–400 °C and slow decomposition at higher temperatures, in similar way as for quercetin alone. Taking into account decomposition processes for pure quercetin and pure Fe_3O_4, it was calculated that quercetin content in the modified Fe_3O_4 sample is around 7.3 weight%, that is comparable to other magnetite nanoparticles coated with small (non-macromolecular) organic molecules.

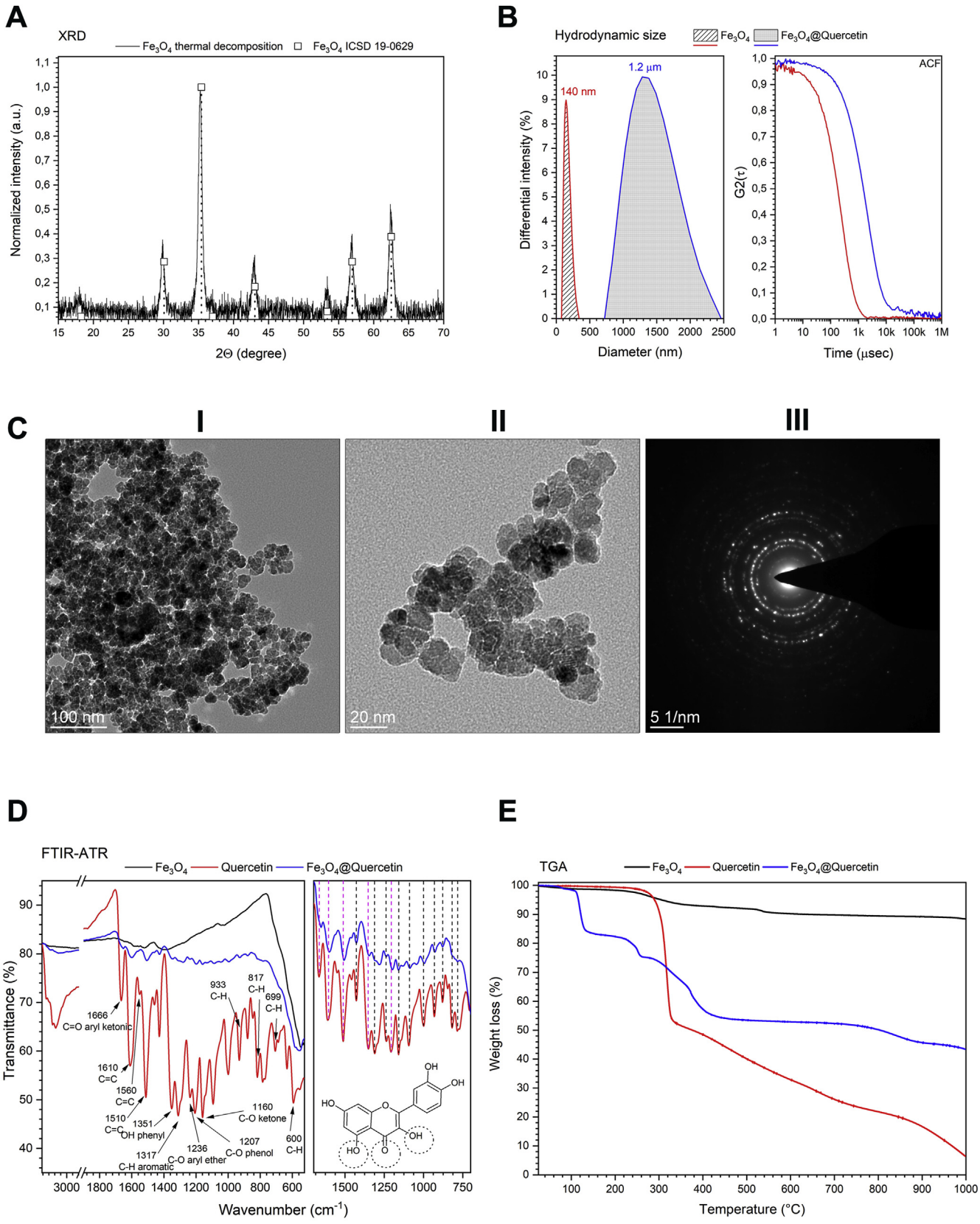

Fig. 1. The characterization of magnetite nanoparticles and quercetin surface functionalized magnetite nanoparticles. (A) X-ray powder diffraction pattern of pure magnetite nanoparticles. (B) Hydrodynamic size of pure and quercetin grafted magnetite nanoparticles (left) and auto-correlation function (right). (C) TEM images of magnetite nanoparticles (I and II) as well as selected area electron diffraction image (III). (D) FTIR-ATR spectra of quercetin surface modified magnetite nanoparticles. (E) TGA analysis of bare magnetite nanoparticles, quercetin, and quercetin surface functionalized magnetite nanoparticles.

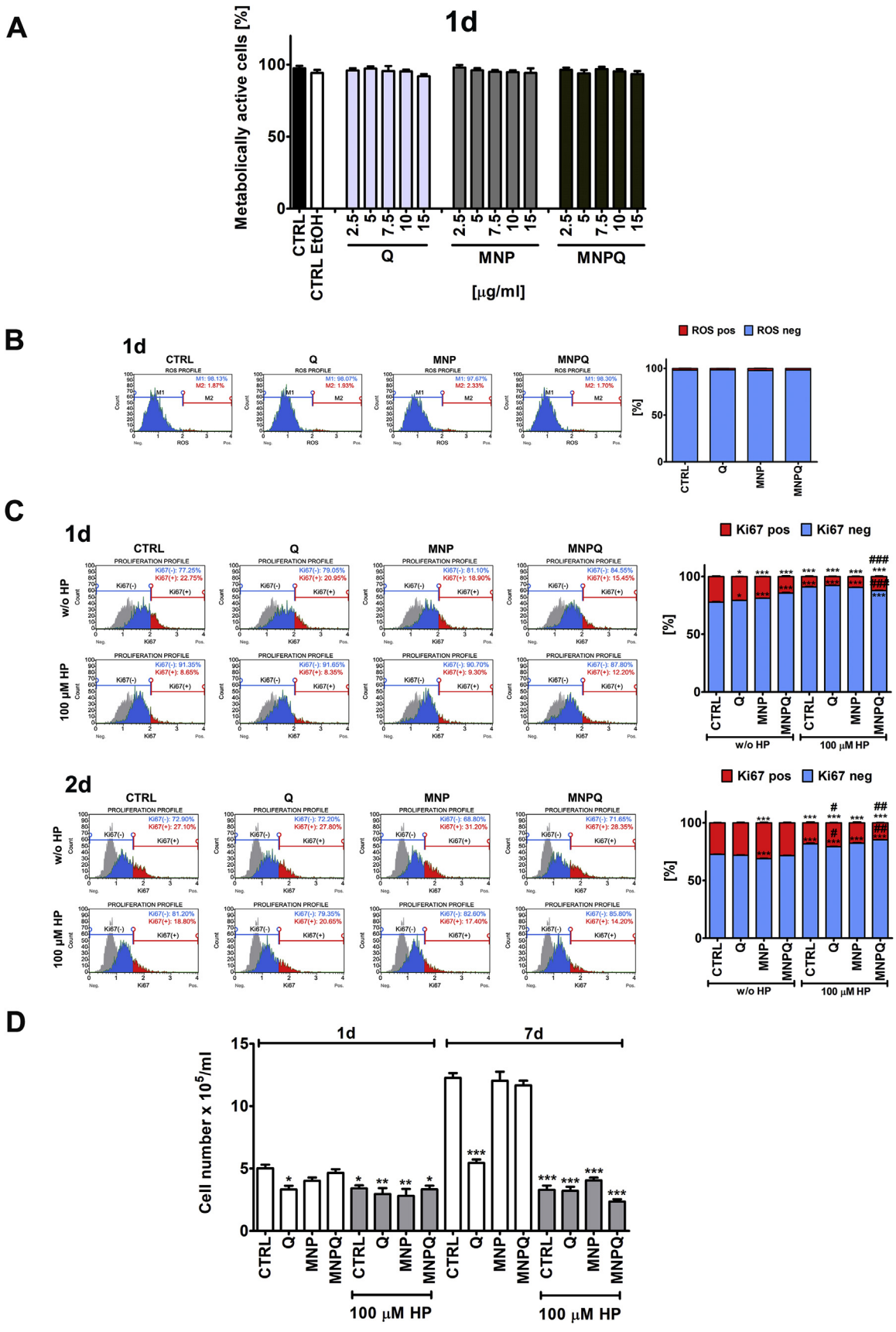

(caption on next page)

Fig. 2. MNPQ-mediated effects on cell proliferation during hydrogen peroxide-induced senescence in BJ human fibroblasts. The concentrations of Q, MNP and MNPQ were selected on the basis of MTT results (A) and reactive oxygen species (ROS) production (B) upon 24 h stimulation with Q, MNP or MNPQ (2.5 to 15 μg/ml). A concentration of 5 μg/ml that did not promote changes in metabolic activity and ROS production was selected for further analysis. (A) The metabolic activity was analyzed using MTT test. Metabolic activity at control conditions (CTRL) is considered as 100%. A solvent action (ethanol) is also shown. (B) Superoxide levels were measured using Muse™ Cell Analyzer and Muse™ Oxidative Stress Kit. Representative histograms are presented. Cell proliferation was measured using Ki67 immunostaining (C) and cell count analysis (D). Cells were stimulated with 100 μM hydrogen peroxide (HP) for 2 h and then cultured in the presence of 5 μg/ml Q, MNP or MNPQ for 24 h, and then culture for up to 168 h without Q, MNP or MNPQ. (C) Cell proliferation was assayed using Muse™ Cell Analyzer and Muse™ Ki67 Proliferation Kit. Representative histograms are presented. A negative control without incubation with Ki67 specific antibody is denoted as a grey histogram in each studied sample. Ki67 immunostaining was analyzed after 24 h treatment with 5 μg/ml Q, MNP or MNPQ. (D) Cell number was analyzed using TC10™ automated cell counter. Bars indicate SD, n = 3, $^{***}p < 0.001$, $^{**}p < 0.01$, $^{*}p < 0.05$ compared to CTRL, $^{\#\#\#}p < 0.001$, $^{\#\#}p < 0.01$, $^{\#}p < 0.05$ compared to HP-treated control (ANOVA and Dunnett's *a posteriori* test). **CTRL**, control conditions; **Q**, quercetin; **MNP**, magnetite nanoparticles; **MNPQ**, quercetin surface functionalized magnetite nanoparticles.

3.2. MNPQ eliminated hydrogen peroxide-induced senescent fibroblasts

First, we have analyzed the effects of Q, MNP and MNPQ on metabolic activity of cells without hydrogen peroxide stimulation (Fig. 2A).

Based on literature data [10], several concentrations of Q, MNP and MNPQ were considered, namely 2.5, 5, 7.5, 10 and 15 μg/ml and 24 h treatment (Fig. 2A). The effect of solvent used (ethanol) was also evaluated (Fig. 2A). There were no statistically significant differences in metabolic activity between control and treated cells (Fig. 2A). As concentration of 5 μg/ml Q, MNP and MNPQ also did not provoke reactive oxygen species (ROS) production (Fig. 2B), thus this concentration was selected for further analysis involving hydrogen peroxide treatment. As MTT test cannot inform us directly about cytotoxic versus cytostatic effects of agents used, several biomarkers of cell proliferation and cytotoxicity were then considered (Figs. 2 and 3, Fig. 4 and Fig. 5). 24 h treatments with Q, MNP and MNPQ transiently lowered the levels of Ki67, a marker of cell proliferation (Fig. 2C), and Q-, MNP- and MNPQ-mediated decrease in cell proliferation was almost not observed upon 48 h of culture (Fig. 2C). As expected, 100 μM hydrogen peroxide (HP, 2 h treatment) inhibited cell proliferation of all categories analyzed both 24 h and 48 h upon hydrogen peroxide removal (Fig. 2C). MNPQ promoted a very slight increase in cell proliferation compared to HP-treated control both 24 h and 48 h upon hydrogen peroxide removal (Fig. 2C). Cell number as a marker of cell proliferation was also quantified using automated cell counter (Fig. 2D). As expected, cell proliferation of all HP-treated cell categories was permanently inhibited upon 7 days of HP removal (Fig. 2D). HP-mediated inhibition of cell proliferation was observed also upon 24 h of HP removal (Fig. 2D). Surprisingly, Q alone diminished cell count (Fig. 2D). HP caused G2/M cell cycle arrest that was the most accented upon 24 h of HP removal (Fig. 3).

MNPQ treatment alone or in combination with HP did not result in specific changes in cell cycle compared to control and HP-treated control, respectively (Fig. 3). The levels of two cell cycle inhibitors, namely p21 and p53 were then analyzed (Fig. 4).

MNP and MNPQ treatments caused an increase in the levels of p21 upon 7 days of HP removal (Fig. 4A). Q alone and in combination with HP also transiently augmented the levels of p21 that was especially observed upon 24 h of HP removal (Fig. 4A). HP-mediated upregulation of p53 was more evident upon 24 h of HP removal than upon 7 days of HP removal (Fig. 4A), but only in HP-treated control and Q-treated cells. MNPQ alone was able to stimulate more potent increase in p53 levels than in combination with HP (Fig. 4A). Changes in intracellular localization of p21 and p53 were also considered (Fig. 4B). Interestingly, imaging flow cytometry revealed that p21 and p53 were not translocated into the nucleus under stress conditions (Fig. 4B). Moreover, more p21 positive cells were found in the cytoplasm after Q and MNPQ treatment under stress conditions and more p53 positive cells were observed in the cytoplasm after MNPQ treatment and in the control (CTRL) after exposure to HP (Fig. 4B).

Except of Q treatment alone and 7 days of culture, Q, MNP or MNPQ treatments without the stimulation with HP did not provoke cytotoxicity as judged by Annexin V staining and dye exclusion assay (Fig. 5).

HP induced apoptotic cell death in all categories analyzed and the pro-apoptotic effect was the most accented upon 7 days of HP removal (Fig. 5A). MNPQ slightly potentiated the pro-apoptotic effect of HP upon 48 h of HP removal compared to HP-treated control (Fig. 5A). However, this was not observed upon 7 days of HP removal (Fig. 5A). Instead, upon 7 days of HP removal, MNPQ promoted non-apoptotic cell death compared to HP-treated control as judged by dye exclusion assay (Fig. 5B). A decrease of about 38% of live cells was noticed after MNPQ treatment compared to HP-treated control (Fig. 5B). This may suggest that MNPQ may help to eliminate stressed cells upon HP stimulation. As HP is a well established inducer of stress-induced premature senescence (SIPS) [28] and 2 h stimulation with 100 μM HP is able to promote SIPS in BJ cells [31], we decided then to analyze MNPQ-mediated levels of senescent cells with and without treatment with HP (Fig. 6A).

Of course, HP treatment resulted in SIPS in BJ cells (Fig. 6A). MNPQ promoted elimination of senescent cells compared to HP-treated cells (Fig. 6A). A decrease of about 38% of senescent cells was observed after MNPQ treatment compared to HP-treated control (Fig. 6A). MNPQ-mediated senolytic effect was statistically significant (Fig. 6A). Unmodified MNP also exerted a senolytic effect, but this was less accented compared to MNPQ-mediated senolytic effect (Fig. 6A). Surprisingly, Q alone induced senescence without HP stimulation (Fig. 6A). However, Q-mediated senolytic effect upon HP stimulation was not noticed (Fig. 6A).

3.3. MNPQ stimulated AMPK activity and lowered secretion of proinflammatory factors during oxidant-induced cellular senescence

As cell cycle arrested senescent cells are considered to be metabolically active cells with affected signal transduction pathways and secretory profiles (e.g., overproduction of pro-inflammatory cytokines) and proteostasis [2,3], we have then analyzed MNPQ-mediated activity of selected kinases namely AMP-activated protein kinase (AMPK) and protein kinase B (PKB, AKT) and the levels of autophagy protein LC3BII, pro-inflammatory agents and some metabolic parameters (Fig. 6B and C, and Fig. 7). During HP-induced cellular senescence in the presence of MNPQ, elevated activity of AMPK (increased ratio of phosphorylated AMPK to AMPK) was observed (Fig. 6B and C). As the activation of AMPK may be a sign of energetic stress and an inducer of autophagy, the levels of autophagy biomarker, namely LC3BII was then assayed (Fig. 6B and C). However, MNPQ-mediated increase in activity of AMPK was not accompanied by elevated levels of LC3BII (Fig. 6B and C). Thus, MNPQ treatment did not promote autophagy during HP-induced cellular senescence. However, autophagy induction was observed after prolonged culture (7 days) and initial 24 treatment with MNPQ alone (Fig. 6B and C). In contrast, MNPQ provoke AMPK-mediated senostatic effect (a decrease in pro-inflammatory agents) during HP-induced premature senescence (Fig. 6B and C). Indeed, MNPQ-associated diminution in the levels of secreted interferon beta (IFN-β) and interleukin 8 (IL-8) (Fig. 6B and C) was observed during oxidant-induced

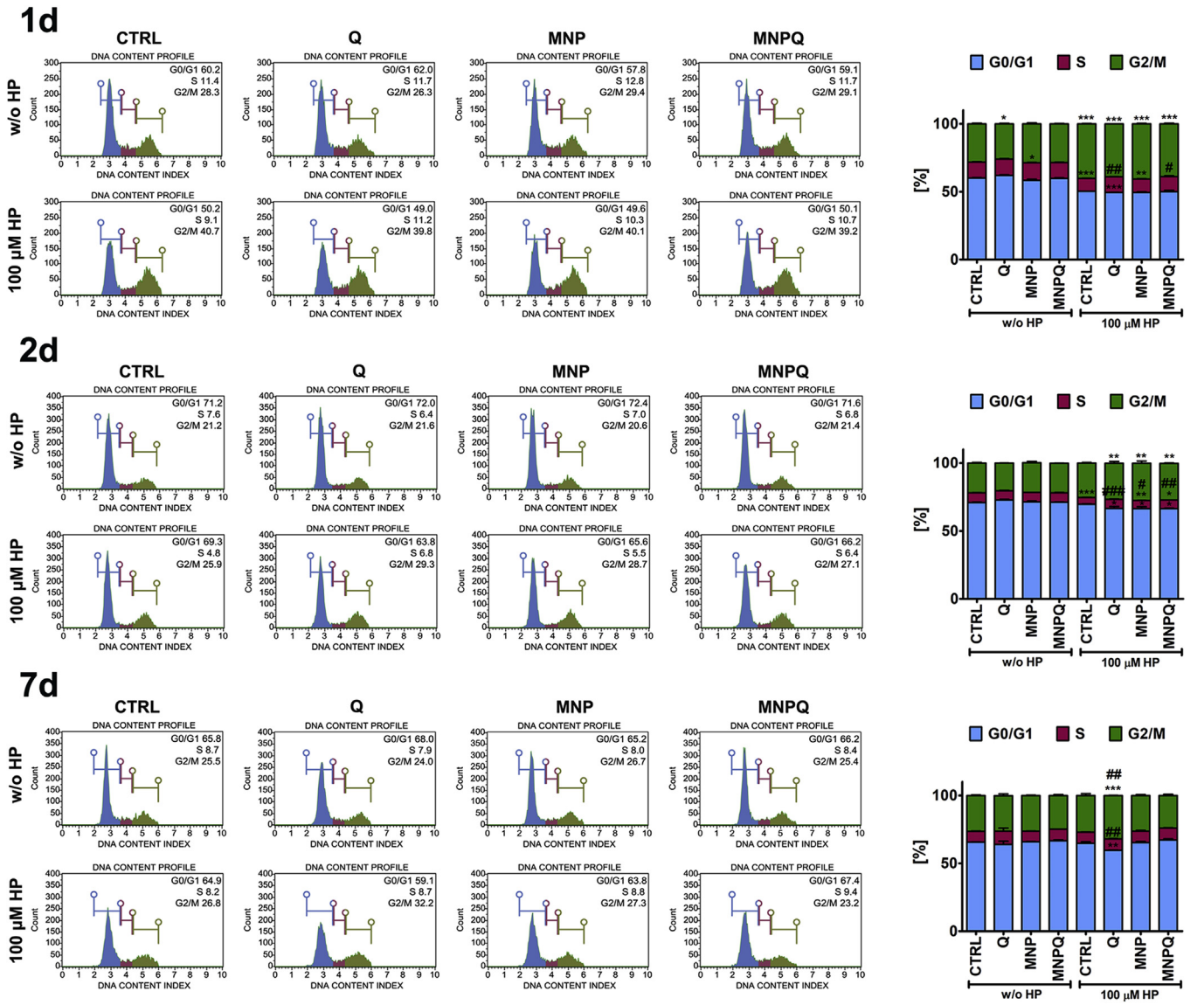

Fig. 3. MNPQ-mediated changes in cell cycle progression. DNA content based analysis of cell cycle was conducted using Muse™ Cell Analyzer and Muse™ Cell Cycle Kit. Representative histograms are presented. Bars indicate SD, n = 3, $^{***}p < 0.001$, $^{**}p < 0.01$, $^{*}p < 0.05$ compared to CTRL, $^{\#\#\#}p < 0.001$, $^{\#\#}p < 0.01$, $^{\#}p < 0.05$ compared to HP-treated control (ANOVA and Dunnett's *a posteriori* test). **CTRL**, control conditions; **Q**, quercetin; **MNP**, magnetite nanoparticles; **MNPQ**, quercetin surface functionalized magnetite nanoparticles.

senescence (Fig. 6B and C). MNPQ also decreased the levels of intracellular IFN-β upon 7 days of HP removal, but similar effect was noticed for Q and MNP (Fig. 6B and C).

3.4. MNPQ-mediated effects on glycolytic pathway and mitochondrial oxidative phosphorylation

In general, HP-induced stress conditions resulted in increased activity of AKT (elevated ratio of phosphorylated AKT to AKT) and augmented levels of glucose transporter GLUT1 (Fig. 6B and C) that may suggest affected glucose uptake and glucose metabolism. To study MNPQ-mediated changes in glucose metabolism more comprehensively, real-time measurements of glycolysis as an extracellular acidification rate (ECAR) and mitochondrial oxidative phosphorylation (OXPHOS) as an oxygen consumption rate (OCR) were considered using an extracellular flux analyzer (Fig. 7).

MNPQ-mediated changes in glycolytic pathway were evaluated by monitoring selected parameters of ECAR, namely glycolysis after the addition of glucose, glycolytic capacity after the addition of oligomycin and glycolytic reserve after the addition of 2-DG (Fig. 7A). HP treatment promoted an increase in all ECAR parameters analyzed (Fig. 7A). MNPQ augmented glycolytic reserve parameter compared to HP-treated control, but similar effect was also observed for unmodified MNP (Fig. 7A). To analyze MNPQ-mediated changes in mitochondrial oxidative phosphorylation (OXPHOS), several parameters of OCR were considered, namely basal respiration, ATP production and proton leak after the addition of oligomycin, maximal respiration after the addition of the uncoupler FCCP and spare respiratory capacity after the addition of rotenone and antimycin A (Fig. 7B). HP treatment induced an increase of selected parameters of OCR, namely basal respiration, maximal respiration and proton leak (Fig. 7B). MNPQ alone also slightly promoted an increase of basal respiration, maximal respiration and proton leak (Fig. 7B). However, HP-associated oxidative stress did not affect ATP production and spare respiratory capacity (Fig. 7B). ATP production was diminished after MNP and MNPQ treatments without HP stimulation (Fig. 7B).

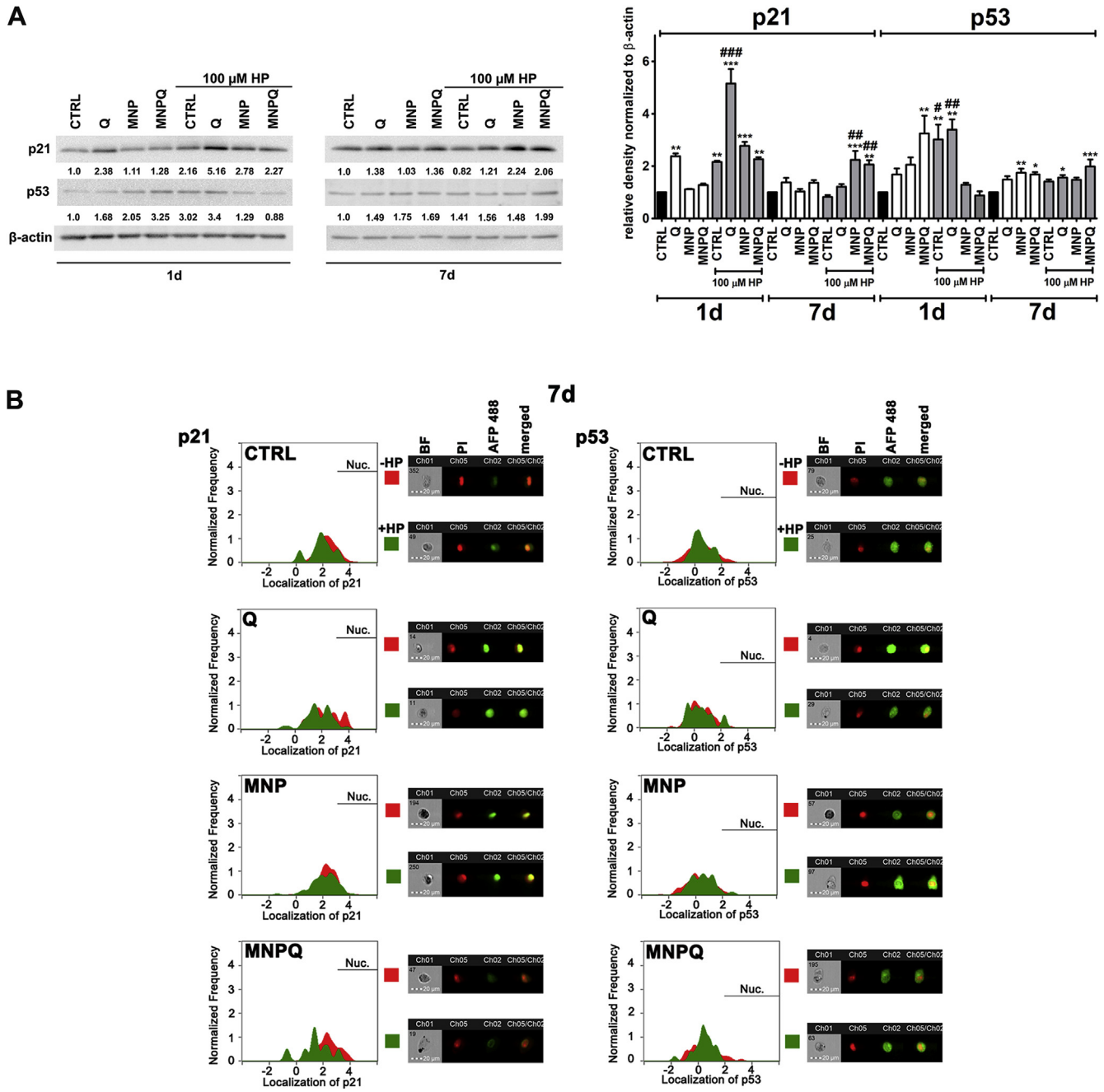

Fig. 4. MNPQ-mediated changes in the levels (A) and localization (B) of cell cycle inhibitors, namely p21 and p53. (A) Western blot analysis of the levels of p21 and p53. Data were normalized to β-actin. (B) Immunofluorescence analysis of cellular localization of p21 and p53. Representative histograms are presented (left). Samples without HP treatment are red and samples with HP treatment are green. Nuclear signals of p21 and p53 are denoted with horizontal lines (Nuc.). Representative images are also shown (right). Ch01, bright field (BF); Ch05, nucleus staining using propidium iodide staining (red, PI); Ch02, immunostaining of p21 and p53 using secondary antibodies conjugated to Alexa Fluor Plus 488 (green, AFP 488); Ch05/Ch02, a merged image of Ch05 and Ch02. Bars indicate SD, n = 3, $^{***}p < 0.001$, $^{**}p < 0.01$, $^{*}p < 0.05$ compared to CTRL, $^{###}p < 0.001$, $^{##}p < 0.01$, $^{#}p < 0.05$ compared to HP-treated control (ANOVA and Dunnett's *a posteriori* test). **CTRL**, control conditions; **Q**, quercetin; **MNP**, magnetite nanoparticles; **MNPQ**, quercetin surface functionalized magnetite nanoparticles. (For interpretation of the references to colour in this figure legend, the reader is referred to the Web version of this article.)

4. Discussion

We have shown for the first time that quercetin surface functionalized magnetite nanoparticles (MNPQ) may promote non-apoptotic cell death and limit the levels of oxidant-induced senescent cells that was accompanied by increased activity of AMP-activated protein kinase (AMPK) and reduced secretion of proinflammatory factors, namely interleukin 8 (IL-8) and interferon beta (IFN-β). Thus, senolytic and senostatic activity of MNPQ was documented in human fibroblasts subjected to stress-induced premature senescence (SIPS) *in vitro* (Fig. 8).

It was already shown that the ferrite based magnetic particles, mainly Fe_3O_4, due to their proven biocompatibility and biodegradability, are attractive in oncological medicine [43,44]. Therefore, development of new multifunctional systems combining magnetic ferrite nanoparticles with anchored hydrophobic drugs is of great importance in modern theranostic applications of cancer treatment [45,46]. This approach allows for construction of smart platforms which functions are directly related to the properties of each constituent. For instance,

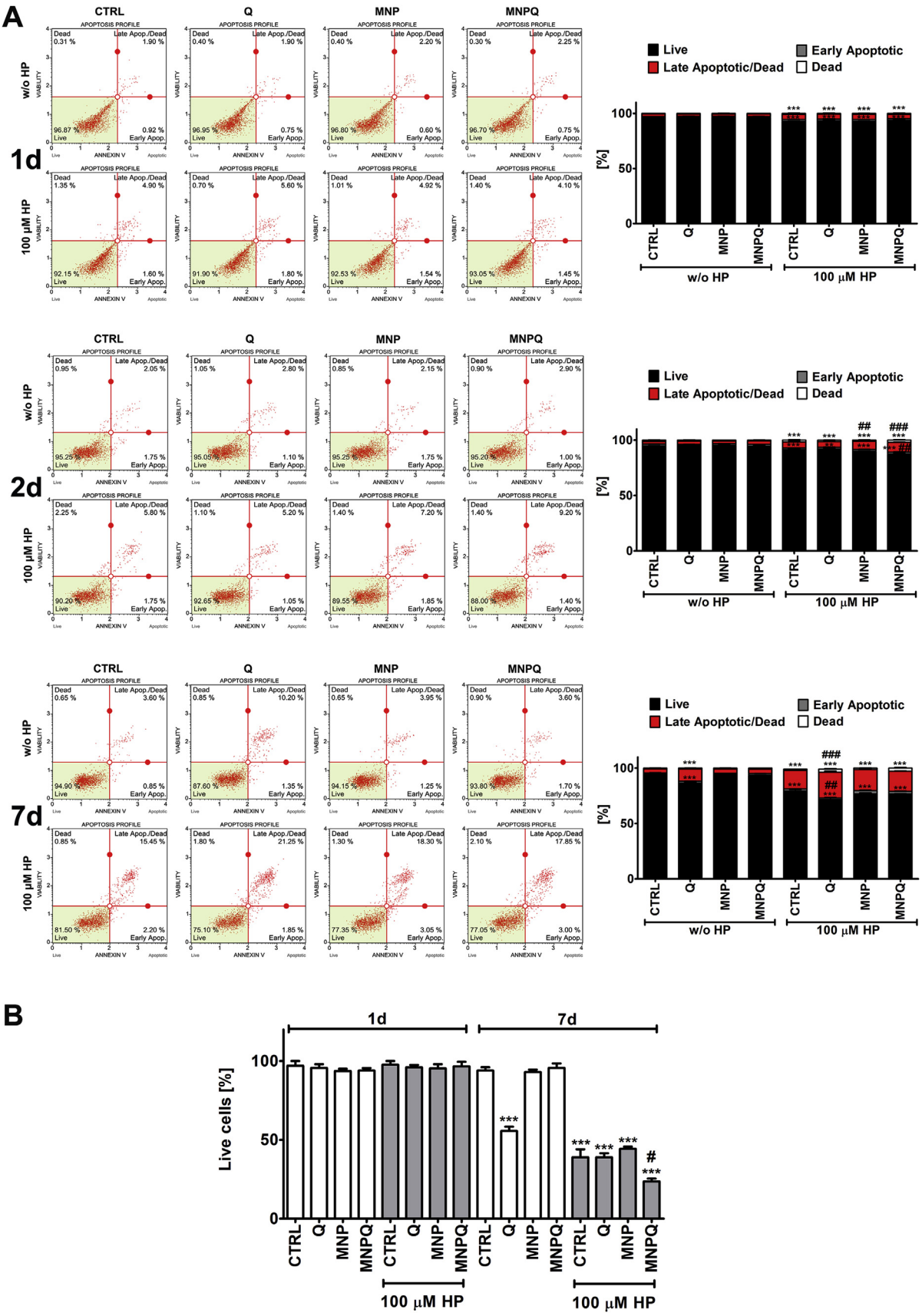

Fig. 5. MNPQ-induced apoptosis (A) and changes in cell membrane permeability (B). (A) Apoptosis was analyzed using Muse™ Cell Analyzer and Muse™ Annexin V and Dead Cell Assay. Representative dot plots are shown. (B) Cell membrane permeability was analyzed using dye exclusion assay using trypan blue staining and TC10™ automated cell counter. Bars indicate SD, n = 3, $^{***}p < 0.001$, $^{**}p < 0.01$ compared to CTRL, $^{\#\#\#}p < 0.001$, $^{\#\#}p < 0.01$, $^{\#}p < 0.05$ compared to HP-treated control (ANOVA and Dunnett's *a posteriori* test). **CTRL**, control conditions; **Q**, quercetin; **MNP**, magnetite nanoparticles; **MNPQ**, quercetin surface functionalized magnetite nanoparticles. (For interpretation of the references to colour in this figure legend, the reader is referred to the Web version of this article.)

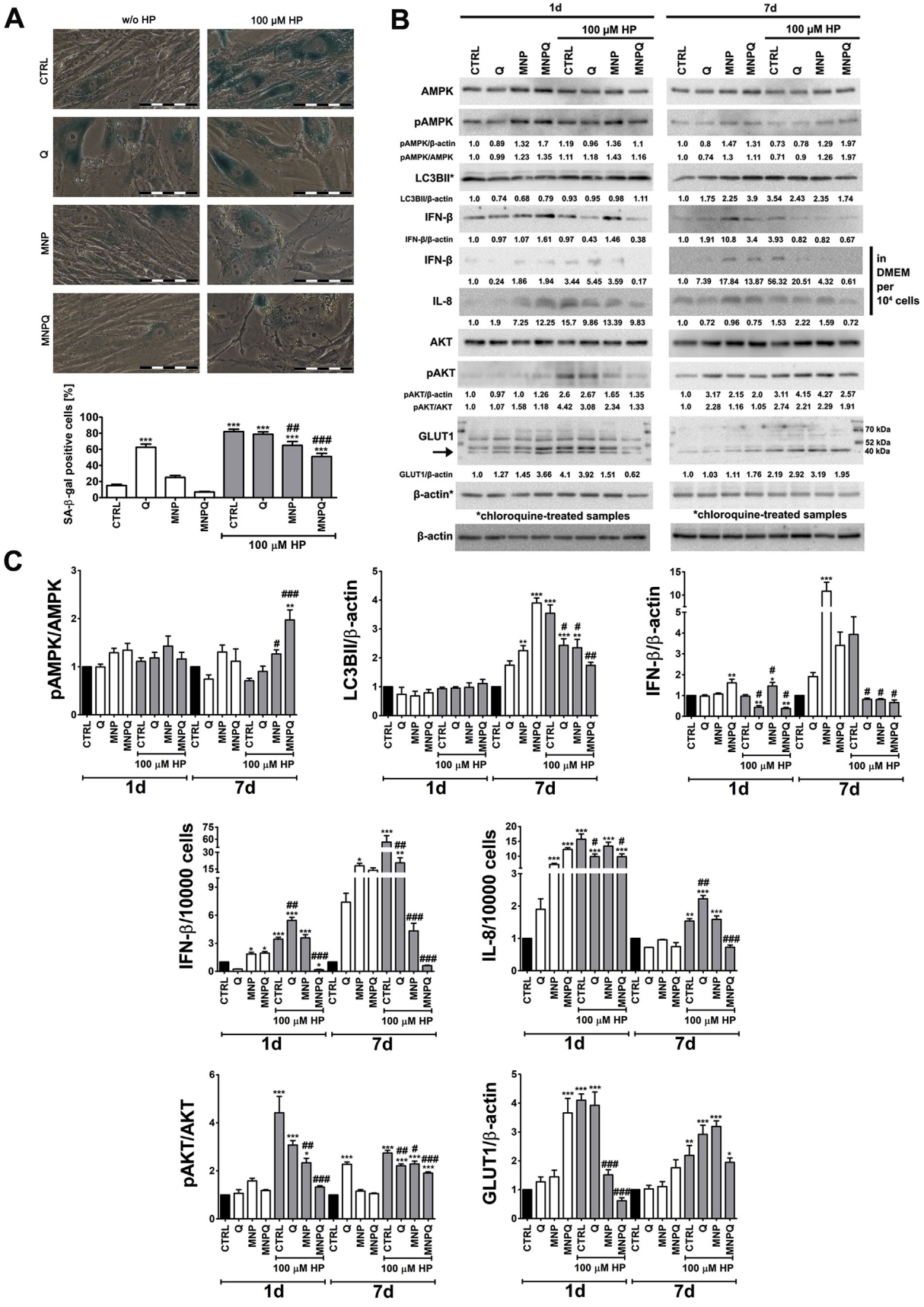

(caption on next page)

Fig. 6. MNPQ-mediated changes in the levels of HP-induced senescent cells (A) and the levels of selected proteins involved in cell signaling, proinflammatory responses, autophagy and glucose uptake (B, C). (A) Senescence-associated β-galactosidase activity. Representative microphotographs are shown. Scale bars 100 μm, objective 20x. (B, C) Western blot analysis of the levels of AMPK, phospho-AMPK, LC3BII, IFN-β, IL-8, AKT, phospho-AKT and GLUT1. For evaluation of LC3BII levels, cells were also incubated with 50 μg/ml chloroquine for 6 h. Data were normalized to β-actin. Chloroquine-treated samples are denoted with an asterisk. The levels of phospho-AMPK and phospho-AKT are also presented as a ratio of phospho-AMPK to AMPK and phospho-AKT to AKT, respectively. IL-8 and IFN-β levels in supernatants were calculated per 10000 cells. Bars indicate SD, n = 3, $^{***}p < 0.001$, $^{**}p < 0.01$, $^{*}p < 0.05$ compared to CTRL, $^{\#\#\#}p < 0.001$, $^{\#\#}p < 0.01$, $^{\#}p < 0.05$ compared to HP-treated control (ANOVA and Dunnett's *a posteriori* test). **CTRL**, control conditions; **Q**, quercetin; **MNP**, magnetite nanoparticles; **MNPQ**, quercetin surface functionalized magnetite nanoparticles.

magnetic particles are already multifunctional because they can be used either as a diagnostic tool in magnetic resonance imaging (contrast) [47] or directly as a therapeutic agent in hyperthermia-based cancer treatment [48]. Another exciting possibility is to exploit magnetic nanoparticles as carriers of hydrophobic drugs. They can be directed towards specific localizations by the static magnetic field and released upon action of alternating magnetic field (heat-triggered drug release) in so called magnetic drug delivery [49]. This is very attractive strategy since the bioavailability of hydrophobic drugs can be significantly altered [50]. However, several challenges were already identified like proper control over particle size distribution, morphology, surface modification, biocompatibility, stability in biological media, controlling target temperature, safe dosage and other factors [51]. Due to above mentioned issues, these specific applications of nanoparticles in living organisms require a careful evaluation of *in vitro* cytotoxicity and particle interaction with different cell lines. It is worth noting that the several systems based on magnetic nanoparticles were successfully studied in humans in due treatment of glioblastoma and prostate carcinoma [52–54].

In general, cellular senescence *in vitro* can be assayed using two paradigms, namely telomere shortening-mediated replicative senescence and stress-induced premature senescence (SIPS) [28,55]. A sublethal dose of hydrogen peroxide (HP) is a well established inducer of SIPS in human fibroblasts *in vitro* [28,31]. Indeed, HP treatment resulted in decreased cell proliferation (Ki67 proliferation marker and cell count), accumulation of cells at G2/M phase of cell cycle and elevated senescence-associated beta-galactosidase activity (this study). HP stimulation also promoted an increase in the levels of cell cycle inhibitors, namely p53 and p21, but they were not translocated into the nucleus. Instead, cytosolic fractions of p53 and p21 were augmented after HP treatment (this study). These observations may suggest other than classical transactivation-dependent effects of p53 during HP-mediated SIPS in the presence of MNPQ in BJ cells. Indeed, the involvement of cytoplasmic p53 in the modulation of apoptosis, autophagy, metabolism, oxidative stress and drug response has been recently established [56,57]. For example, cytoplasmic activated p53 can bind a pro-apoptotic protein Bax and facilitate its mitochondrial translocation and homo-oligomerization that in turn may lead to mitochondrial membrane permeabilization, cytochrome *c* release and apoptotic cell death [56,57]. Moreover, oxidative stress may stimulate p53 activation and its mitochondrial translocation that may result in the interactions between p53 and cyclophilin D in the mitochondrial matrix leading to

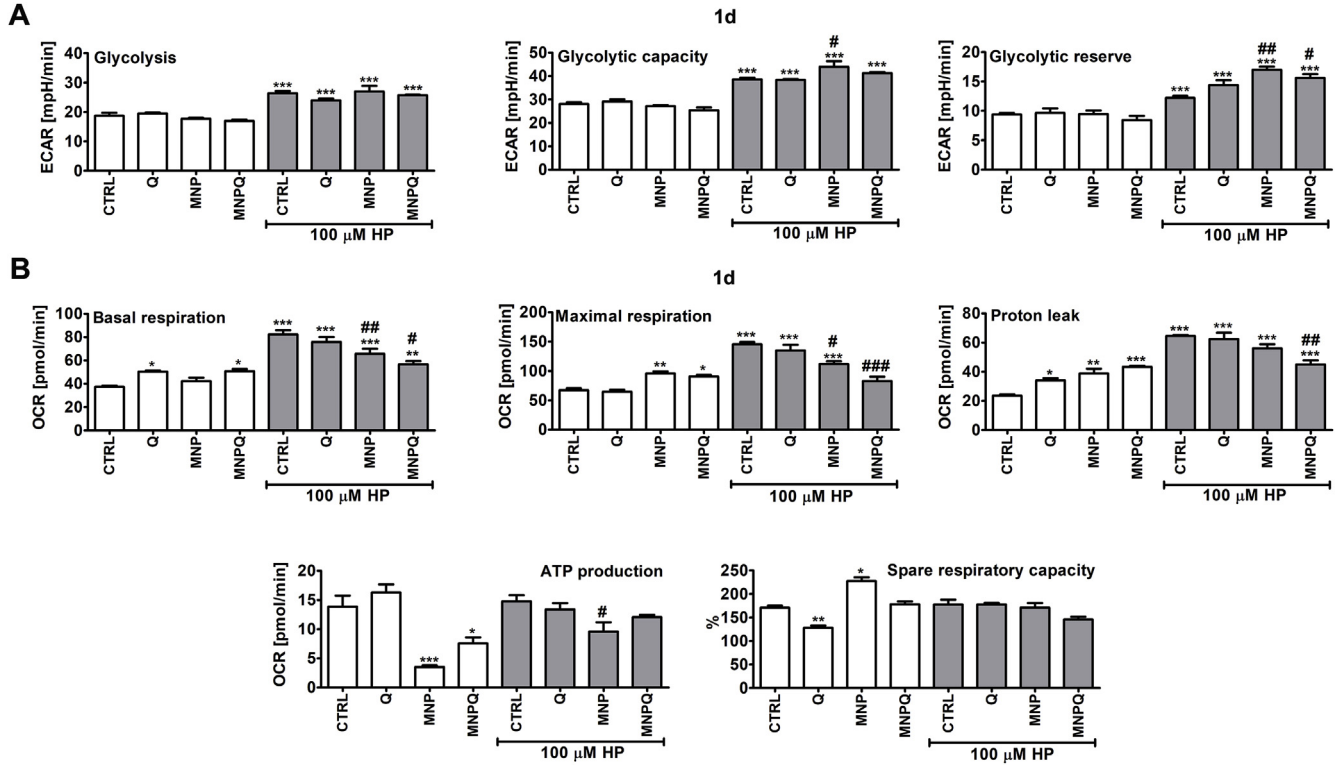

Fig. 7. MNPQ-mediated effects on selected parameters of extracellular acidification rate (ECAR, Glycolysis Stress Test) (A) and oxygen consumption rate (OCR, Cell Mito Stress Test) (B). (A) Real-time measurements of glycolysis as ECAR parameters (from left to right): glycolysis after the addition of glucose, glycolytic capacity after the addition of oligomycin and glycolytic reserve after the addition of 2-DG. (B) Real-time measurements of mitochondrial oxidative phosphorylation (OXPHOS) as OCR parameters: basal respiration, ATP production and proton leak after the addition of oligomycin, maximal respiration after the addition of the uncoupler FCCP and spare respiratory capacity after the addition of rotenone and antimycin A. ECAR and OCR were measured using an extracellular flux analyzer (Seahorse XFp Analyzer). Bars indicate SD, n = 3, $^{***}p < 0.001$, $^{**}p < 0.01$ compared to CTRL, $^{\#\#}p < 0.01$, $^{\#}p < 0.05$ compared to HP-treated control (ANOVA and Dunnett's *a posteriori* test). **CTRL**, control conditions; **Q**, quercetin; **MNP**, magnetite nanoparticles; **MNPQ**, quercetin surface functionalized magnetite nanoparticles.

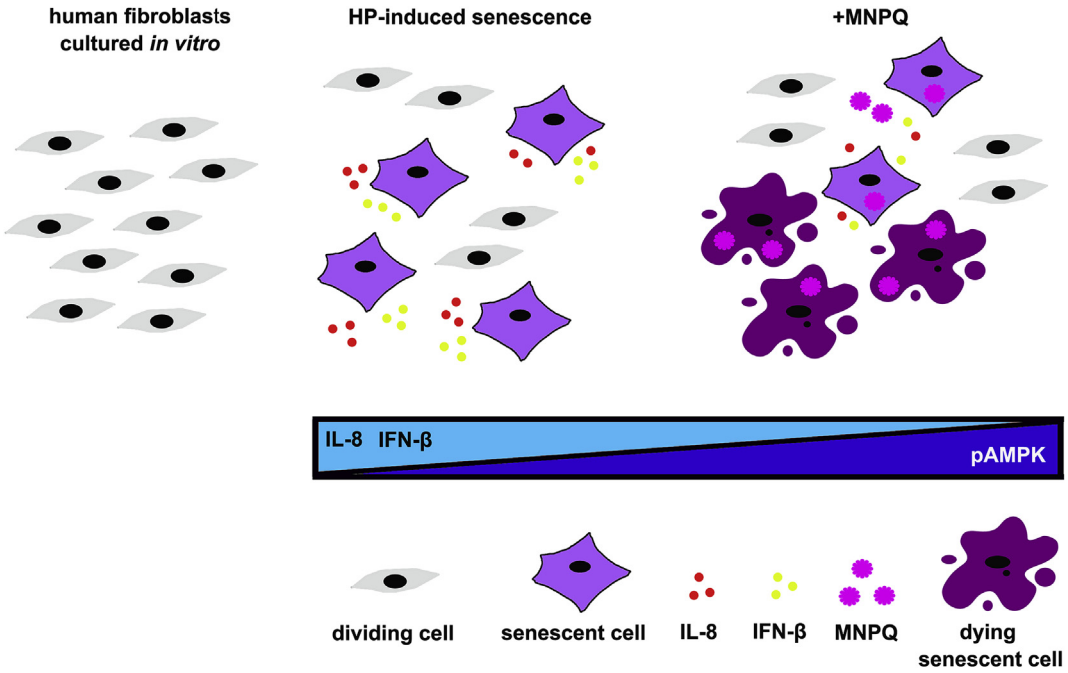

Fig. 8. MNPQ-mediated senolytic and senostatic activity during hydrogen peroxide-promoted senescence in BJ human fibroblasts *in vitro*. MNPQ treatment resulted in the elimination of oxidant-induced senescent cells (senolytic action) and suppression of proinflammatory responses (decreased secretion of IL-8 as a part of SASP response and decreased secretion of IFN-β as a part of interferon response) (senostatic action). The observed effects were accompanied by increased activity of AMPK (increased ratio of phosphorylated AMPK to AMPK).

mitochondrial inner membrane protein VDAC oligomerization, mitochondrial permeability transition pore (PTP) formation and necrotic cell death [57]. The activation of cytoplasmic p53 may also inhibit glycolysis and pentose phosphate pathway and promote oxidative stress and suppress the autophagic pathway [57]. Cellular localization of p21 may also determine its biological functions [58]. Nuclear p21 may promote DNA damage-induced cell cycle arrest and act as a tumor suppressor, whereas cytoplasmic p21 may possess anti-apoptotic activity and act as an oncogene [58].

Surprisingly, MNPQ treatment resulted in decreased number of senescent cells during HP-mediated SIPS that was due to elevated levels of dead cells as judged by dye exclusion assay. As the levels of apoptotic cells upon MNPQ stimulation were increased of about 4% compared to untreated control, one can conclude that MNPQ did not eliminate senescent cells by the means of apoptotic cell death. Instead, non-apoptotic mode of death with affected cell membrane permeability was observed. However, we did not analyze further if MNPQ induced necrotic or regulated necroptotic cell death. In general, senescent cells are considered to be resistant to apoptosis due to upregulation of senescent-cell anti-apoptotic pathways (SCAPs) [17]. It has been reported that targeting SCAPs using co-treatment with dasatinib and quercetin or Bcl-2 inhibitors promoted apoptosis of some but not all senescent cell types [10,11,18]. Senotherapeutic action of natural products may be also considered cell-type specific. Indeed, fisetin stimulated apoptosis in HUVECs, whereas in MEFs, fisetin lowered the levels of senescent cells without evidence of cell killing [18]. Moreover, senolytic activity of quercetin in senescent HUVECs was observed, whereas neither quercetin nor the 3-O-galactoside of quercetin (hyperoside) were effective against senescent adult endothelial cells (EC) *in vitro* [59]. Geroprotective effects of quercetin have been also revealed during replicative senescence in human mesenchymal stem cells (hMSCs) and using a premature aging model, namely Werner syndrome (WS) hMSCs [60]. Plant-derived natural substances are considered to be promising candidates for senolytic-based anti-aging therapies as they are less toxic than targeted therapeutics with senolytic activity [16]. However, in some instances, natural products must be combined with other senolytic agents to show potent senolytic effects as have been already documented for co-treatment with dasatinib and quercetin [10].

It is widely accepted that the action of AMP-activated protein kinase (AMPK) is not limited to the maintenance of energy metabolism but AMPK may also modulate the aging process by an integrated signaling network [61,62]. AMPK activity may promote healthspan and lifespan by providing cellular stress resistance by stimulation of FoxO/DAF-16, Nrf2/SKN-1 and SIRT1 signaling pathways, autophagic clearance through mTOR and ULK1 signaling and suppression of proinflammatory responses by inhibition of NF-κB signaling [61,62]. Indeed, it has been repeatedly reported that increased AMPK activity may extend the lifespan of lower organisms and AMPK activity declines with aging [62]. More recently, it has been documented that the deletion of AMPKα2, but not AMPKα1 promoted cellular senescence and cell cycle arrest in MEFs that was mediated by oxidative stress-induced upregulation of p16 [63]. Elevated AMPK activity was also revealed upon stimulation with MNPQ during hydrogen peroxide-induced senescence in BJ fibroblasts that was accompanied by decreased secretion of IL-8 and IFN-β (this study). Senescent cells are characterized by senescence-associated secretory phenotype (SASP) and SASP components may include proinflammatory and immune-modulatory cytokines and chemokines (e.g., IL-6, IL-7, IL-8, MCP-2, MIP-3a), growth factors (e.g., GRO, HGF, IGFBPs), cell surface molecules (e.g., ICAMs, uPAR, TNF receptors) and survival factors [3,64]. More recently, it has been documented that SASP response is a phenotype of early senescence (replicative senescence), whereas L1 retrotransposable element-mediated interferon response is a phenotype of late senescence that contributes to the maintenance of SASP in human fibroblasts [29]. Interferon response was also observed during oncogene-induced senescence (OIS) and SIPS in human fibroblasts [29]. IL-8 (a part of SASP response) and IFN-β (a part of interferon response) secretion was also elevated during hydrogen peroxide-induced senescence in BJ fibroblasts and MNPQ were able to suppress these proinflammatory responses by the activation of AMPK (this study). SASP may affect neighbouring cells e.g., by the induction of tumorigenesis [1]. Moreover, age-related metabolic diseases such as obesity, type 2 diabetes and atherosclerosis are accompanied by chronic

inflammation associated with elevated NF-κB signaling and impaired AMPK activity, and chronic low-grade inflammation is suggested to be a key factor in the initiation, propagation and development of metabolic disorders [65,66]. AMPK may inhibit NF-κB signaling indirectly by its downstream mediators, e.g., SIRT1, Forkhead box O (FoxO) family, and peroxisome proliferator-activated receptor γ co-activator 1α (PGC-1α) that in turn diminish the expression of proinflammatory agents [61]. The secretion of IL-8 was elevated during cigarette smoke-induced lung inflammation and emphysema in AMPKα1-deficient (AMPKα1-HT) mice and an activator of AMPK decreased the levels of IL-8, whereas an inhibitor of AMPK augmented the levels of IL-8. Similar effects were also observed in A549 human lung cancer cells subjected to cigarette smoke extract (CSE) [67]. AMPK also suppressed pro-inflammatory response, cellular senescence and lung injury in experimentally-induced pulmonary emphysema [68]. Induction of AMPK activity by metformin administration lowered pro-inflammatory cytokine release (keratinocyte chemoattractant, KC and monocytes chemoattractant protein 1, MCP-1) in bronchoalveolar lavage (BAL) fluid in mouse elastase-induced lung emphysema model [68]. Moreover, stimulation of activity of AMPK using a specific AMPK activator (AICAR) resulted in reduced secretion of IL6 and IL-8 by CSE-treated human bronchial epithelial cells (BEAS-2B) and small airway epithelial cells (SAECs) [68].

As proteostasis may be impaired during cellular senescence [3] and AMPK is a well established inducer of autophagy [69], we have then addressed the question of whether MNPQ-mediated increase in AMPK activity may also promote autophagy during SIPS in human fibroblasts. However, MNPQ-induced activity of AMPK was not accompanied by increased levels of LC3BII, a biomarker of autophagy and perhaps MNPQ were not able to stimulate autophagic adaptive response during oxidative stress conditions (this study). More recently, it has been reported that pharmacological activation of AMPK by metformin and berberine counteracted hydrogen peroxide-induced impairment of the autophagic flux in senescent fibroblast cells as judged by decreased p62 degradation, GFP-RFP-LC3 cancellation, and activity of lysosomal hydrolases [70]. The authors concluded that AMPK activation protected oxidative stress-induced senescent fibroblasts by autophagic flux restoration [70].

It is widely accepted that senescent cells are metabolically active [3], but it is still a debate if senescence-associated metabolomic changes are a cause or a consequence of several other hallmarks of senescent cells [71,72]. Senescent cells are characterized by elevated ratios of AMP to ATP and ADP to ATP that may result in the activation of AMPK, a master regulator of cellular responses to energy stress [71]. Increased activation of AMPK may stimulate fatty acid oxidation, mitochondrial biogenesis and glucose uptake, thus AMPK may promote metabolic reprogramming during cellular senescence [73]. Data on metabolic patterns during replicative senescence and SIPS are scarce [74–76]. The analysis of extracellular senescence metabolomes (ESMs) has revealed that glycolytic pathway is elevated during replicative senescence and SIPS in human fibroblasts [75]. Moreover, using a metabolomics−proteomics combined approach and doxorubicin-treated human MCF-7 breast cancer cells as a model of SIPS, the upregulation of tricarboxylic acid cycle, pentose phosphate pathway and nucleotide synthesis pathways was observed [76]. Indeed, real-time measurements of glycolysis as an extracellular acidification rate (ECAR) and mitochondrial oxidative phosphorylation (OXPHOS) as an oxygen consumption rate (OCR) also shown an increase of ECAR and OCR parameters during hydrogen peroxide-induced senescence in BJ human fibroblasts (this study). However, except of MNPQ-mediated decrease in proton leak, there were no specific MNPQ-associated changes in glycolytic pathway and oxidative phosphorylation under oxidative stress conditions. As protein kinase B (AKT) was activated (increased ratio of phosphorylated AKT to AKT) and the levels of glucose transporter 1 (GLUT1) were elevated during oxidant-induced senescence in BJ cells (this study), one can conclude that senescence-associated increase in glucose metabolic pathway was mediated by increased AKT activity. Similarly, AKT hiperactivation in cancer cells may promote aerobic glycolysis and cell proliferation by elevated expression of glucose transporters and activity of selected glycolytic enzymes [77,78].

In conclusion, senolytic and senostatic activity of quercetin surface functionalized magnetite nanoparticles (MNPQ) has been documented (Fig. 8). MNPQ eliminated hydrogen peroxide-induced senescent human fibroblasts and limited senescence-associated proinflammatory responses (decreased secretion of IL-8 and IFN-β) that was mediated by increased AMPK activity. We suggest that MNPQ may be considered as a novel and promising nanoparticle-based strategy to limit the number of senescent cells and thus protect against age-related diseases.

Author contributions

Conceived and designed the experiments: AL, MW, RP. Preparation and characterization of the magnetite nanoparticles: MKG, GL, AT, RP. Performed the experiments: AL, JAG, DB, JO, MW. Analyzed the data: AL, MW, RP. Contributed reagents/materials/analysis tools: AL, MW, RP. Wrote the paper: AL, RP, MW.

Declaration of competing interest

The authors declare that they have no known competing financial interests or personal relationships that could have appeared to influence the work reported in this paper.

Acknowledgments

Financial support of the National Science Centre in course of realization of the Project no. UMO-2017/25/B/ST5/00497 is gratefully acknowledged. Jakub Olszowka is a student of Biotechnology at University of Rzeszow, Poland.

References

[1] F. Rodier, J. Campisi, Four faces of cellular senescence, J. Cell Biol. 192 (2011) 547–556.
[2] C. Lopez-Otin, M.A. Blasco, L. Partridge, M. Serrano, G. Kroemer, The hallmarks of aging, Cell 153 (2013) 1194–1217.
[3] A. Hernandez-Segura, J. Nehme, M. Demaria, Hallmarks of cellular senescence, Trends Cell Biol. 28 (2018) 436–453.
[4] B.I. Pereira, O.P. Devine, M. Vukmanovic-Stejic, E.S. Chambers, P. Subramanian, N. Patel, et al., Senescent cells evade immune clearance via HLA-E-mediated NK and CD8(+) T cell inhibition, Nat. Commun. 10 (2019) 2387.
[5] B.G. Childs, M. Gluscevic, D.J. Baker, R.M. Laberge, D. Marquess, J. Dananberg, et al., Senescent cells: an emerging target for diseases of ageing, Nat. Rev. Drug Discov. 16 (2017) 718–735.
[6] R.M. Naylor, D.J. Baker, J.M. van Deursen, Senescent cells: a novel therapeutic target for aging and age-related diseases, Clin. Pharmacol. Ther. 93 (2013) 105–116.
[7] D.J. Baker, T. Wijshake, T. Tchkonia, N.K. LeBrasseur, B.G. Childs, B. van de Sluis, et al., Clearance of p16Ink4a-positive senescent cells delays ageing-associated disorders, Nature 479 (2011) 232–236.
[8] D.J. Baker, B.G. Childs, M. Durik, M.E. Wijers, C.J. Sieben, J. Zhong, et al., Naturally occurring p16(Ink4a)-positive cells shorten healthy lifespan, Nature 530 (2016) 184–189.
[9] B.G. Childs, D.J. Baker, T. Wijshake, C.A. Conover, J. Campisi, J.M. van Deursen, Senescent intimal foam cells are deleterious at all stages of atherosclerosis, Science 354 (2016) 472–477.
[10] Y. Zhu, T. Tchkonia, T. Pirtskhalava, A.C. Gower, H. Ding, N. Giorgadze, et al., The Achilles' heel of senescent cells: from transcriptome to senolytic drugs, Aging Cell 14 (2015) 644–658.
[11] J. Chang, Y. Wang, L. Shao, R.M. Laberge, M. Demaria, J. Campisi, et al., Clearance of senescent cells by ABT263 rejuvenates aged hematopoietic stem cells in mice, Nat. Med. 22 (2016) 78–83.
[12] R. Yosef, N. Pilpel, R. Tokarsky-Amiel, A. Biran, Y. Ovadya, S. Cohen, et al., Directed elimination of senescent cells by inhibition of BCL-W and BCL-XL, Nat. Commun. 7 (2016) 11190.
[13] Y. Zhu, T. Tchkonia, H. Fuhrmann-Stroissnigg, H.M. Dai, Y.Y. Ling, M.B. Stout, et al., Identification of a novel senolytic agent, navitoclax, targeting the Bcl-2 family of anti-apoptotic factors, Aging Cell 15 (2016) 428–435.
[14] H. Fuhrmann-Stroissnigg, Y.Y. Ling, J. Zhao, S.J. McGowan, Y. Zhu, R.W. Brooks, et al., Identification of HSP90 inhibitors as a novel class of senolytics, Nat. Commun. 8 (2017) 422.
[15] M.P. Baar, R.M.C. Brandt, D.A. Putavet, J.D.D. Klein, K.W.J. Derks, B.R.M. Bourgeois, et al., Targeted apoptosis of senescent cells restores tissue homeostasis in response to chemotoxicity and aging, Cell 169 (2017) 132–147

e116.
[16] W. Li, L. Qin, R. Feng, G. Hu, H. Sun, Y. He, et al., Emerging senolytic agents derived from natural products, Mech. Ageing Dev. 181 (2019) 1–6.
[17] J.L. Kirkland, T. Tchkonia, Y. Zhu, L.J. Niedernhofer, P.D. Robbins, The clinical potential of senolytic drugs, J. Am. Geriatr. Soc. 65 (2017) 2297–2301.
[18] Y. Zhu, E.J. Doornebal, T. Pirtskhalava, N. Giorgadze, M. Wentworth, H. Fuhrmann-Stroissnigg, et al., New agents that target senescent cells: the flavone, fisetin, and the BCL-XL inhibitors, A1331852 and A1155463, Aging (Albany NY) 9 (2017) 955–963.
[19] M.J. Yousefzadeh, Y. Zhu, S.J. McGowan, L. Angelini, H. Fuhrmann-Stroissnigg, M. Xu, et al., Fisetin is a senotherapeutic that extends health and lifespan, EBioMedicine 36 (2018) 18–28.
[20] Y. Wang, J. Chang, X. Liu, X. Zhang, S. Zhang, D. Zhou, et al., Discovery of piperlongumine as a potential novel lead for the development of senolytic agents, Aging (Albany NY) 8 (2016) 2915–2926.
[21] W. Li, Y. He, R. Zhang, G. Zheng, D. Zhou, The curcumin analog EF24 is a novel senolytic agent, Aging (Albany NY) 11 (2019) 771–782.
[22] S. Andres, S. Pevny, R. Ziegenhagen, N. Bakhiya, B. Schafer, K.I. Hirsch-Ernst, et al., Safety aspects of the use of quercetin as a dietary supplement, Mol. Nutr. Food Res. 62 (2018) 1700447.
[23] G.S. Kelly, Quercetin. Monograph, Altern. Med. Rev. 16 (2011) 172–194.
[24] G. D'Andrea, Quercetin, A flavonol with multifaceted therapeutic applications? Fitoterapia 106 (2015) 256–271.
[25] B.B. Aggarwal, S. Shishodia, Molecular targets of dietary agents for prevention and therapy of cancer, Biochem. Pharmacol. 71 (2006) 1397–1421.
[26] W. Wang, C. Sun, L. Mao, P. Ma, F. Liu, J. Yang, et al., The biological activities, chemical stability, metabolism and delivery systems of quercetin: a review, Trends Food Sci. Technol. 56 (2016) 21–38.
[27] D. Munoz-Espin, M. Rovira, I. Galiana, C. Gimenez, B. Lozano-Torres, M. Paez-Ribes, et al., A versatile drug delivery system targeting senescent cells, EMBO Mol. Med. 10 (2018).
[28] O. Toussaint, E.E. Medrano, T. von Zglinicki, Cellular and molecular mechanisms of stress-induced premature senescence (SIPS) of human diploid fibroblasts and melanocytes, Exp. Gerontol. 35 (2000) 927–945.
[29] M. De Cecco, T. Ito, A.P. Petrashen, A.E. Elias, N.J. Skvir, S.W. Criscione, et al., L1 drives IFN in senescent cells and promotes age-associated inflammation, Nature 566 (2019) 73–78.
[30] R. Pazik, R. Tekoriute, S. Hakansson, R. Wiglusz, W. Strek, G.A. Seisenbaeva, et al., Precursor and solvent effects in the nonhydrolytic synthesis of complex oxide nanoparticles for bioimaging applications by the ether elimination (Bradley) reaction, Chemistry 15 (2009) 6820–6826.
[31] A. Lewinska, J. Adamczyk-Grochala, E. Kwasniewicz, A. Deregowska, E. Semik, T. Zabek, et al., Reduced levels of methyltransferase DNMT2 sensitize human fibroblasts to oxidative stress and DNA damage that is accompanied by changes in proliferation-related miRNA expression, Redox Biol 14 (2018) 20–34.
[32] A. Lewinska, P. Jarosz, J. Czech, I. Rzeszutek, A. Bielak-Zmijewska, W. Grabowska, et al., Capsaicin-induced genotoxic stress does not promote apoptosis in A549 human lung and DU145 prostate cancer cells, Mutat. Res. Genet. Toxicol. Environ. Mutagen. 779 (2015) 23–34.
[33] A. Lewinska, A. Bocian, V. Petrilla, J. Adamczyk-Grochala, K. Szymura, W. Hendzel, et al., Snake venoms promote stress-induced senescence in human fibroblasts, J. Cell. Physiol. 234 (2019) 6147–6160.
[34] A. Lewinska, J. Adamczyk-Grochala, E. Kwasniewicz, A. Deregowska, M. Wnuk, Ursolic acid-mediated changes in glycolytic pathway promote cytotoxic autophagy and apoptosis in phenotypically different breast cancer cells, Apoptosis 22 (2017) 800–815.
[35] H.P. Klug, L.E. Alexander, X-Ray Diffraction Procedures: for Polycrystalline and Amorphous Materials, John Wiley and Sons, Inc., New York, 1954.
[36] R. Pązik, E. Piasecka, M. Małecka, V.G. Kessler, B. Idzikowski, Z. Śniadecki, et al., Facile non-hydrolytic synthesis of highly water dispersible, surfactant free nanoparticles of synthetic MFe_2O_4 ($M–Mn^{2+}$, Fe^{2+}, Co^{2+}, Ni^{2+}) ferrite spinel by a modified Bradley reaction, RSC Adv. 3 (2013) 12230–12243.
[37] M. Heneczkowski, M. Kopacz, D. Nowak, A. Kuzniar, Infrared spectrum analysis of some flavonoids, Acta Pol. Pharm. 58 (2001) 415–420.
[38] M. Catauro, F. Papale, F. Bollino, S. Piccolella, S. Marciano, P. Nocera, et al., Silica/quercetin sol-gel hybrids as antioxidant dental implant materials, Sci. Technol. Adv. Mater. 16 (2015) 035001.
[39] B. Pawlikowska-Pawlega, H. Dziubinska, E. Krol, K. Trebacz, A. Jarosz-Wilkolazka, R. Paduch, et al., Characteristics of quercetin interactions with liposomal and vacuolar membranes, Biochim. Biophys. Acta 1838 (2014) 254–265.
[40] R. Enteshari Najafabadi, N. Kazemipour, A. Esmaeili, S. Beheshti, S. Nazifi, Using superparamagnetic iron oxide nanoparticles to enhance bioavailability of quercetin in the intact rat brain, BMC Pharmacol Toxicol 19 (2018) 59.
[41] V.G. Kessler, G.I. Spijksma, G.A. Seisenbaeva, S. Håkansson, D.H.A. Blank, H.J.M. Bouwmeester, New insight in the role of modifying ligands in the sol-gel processing of metal alkoxide precursors: a possibility to approach new classes of materials, J. Sol. Gel Sci. Technol. 40 (2006) 163–179.
[42] V.G. Kessler, The chemistry behind the sol–gel synthesis of complex oxide nanoparticles for bio-imaging applications, J. Sol. Gel Sci. Technol. 51 (2009) 264.
[43] R.A. Revia, M. Zhang, Magnetite nanoparticles for cancer diagnosis, treatment, and treatment monitoring: recent advances, Mater. Today 19 (2016) 157–168.
[44] R. Weissleder, D.D. Stark, B.L. Engelstad, B.R. Bacon, C.C. Compton, D.L. White, et al., Superparamagnetic iron oxide: pharmacokinetics and toxicity, AJR Am. J. Roentgenol. 152 (1989) 167–173.
[45] K.V. Jardim, A.F. Palomec-Garfias, B.Y.G. Andrade, J.A. Chaker, S.N. Bao, C. Marquez-Beltran, et al., Novel magneto-responsive nanoplatforms based on $MnFe_2O_4$ nanoparticles layer-by-layer functionalized with chitosan and sodium alginate for magnetic controlled release of curcumin, Mater Sci Eng C Mater Biol Appl 92 (2018) 184–195.
[46] M. Wu, S. Huang, Magnetic nanoparticles in cancer diagnosis, drug delivery and treatment, Mol Clin Oncol 7 (2017) 738–746.
[47] K.M. Krishnan, Biomedical Nanomagnetics, A spin through possibilities in imaging, diagnostics, and therapy, IEEE Trans. Magn. 46 (2010) 2523–2558.
[48] H.B. Na, I.C. Song, T. Hyeon, Inorganic nanoparticles for MRI contrast agents, Adv. Mater. 21 (2009) 2133–2148.
[49] W. Fan, B. Yung, P. Huang, X. Chen, Nanotechnology for multimodal synergistic cancer therapy, Chem. Rev. 117 (2017) 13566–13638.
[50] K.T. Yong, I. Roy, M.T. Swihart, P.N. Prasad, Multifunctional nanoparticles as biocompatible targeted probes for human cancer diagnosis and therapy, J. Mater. Chem. 19 (2009) 4655–4672.
[51] P. Chen, H. Song, S. Yao, X. Tu, M. Su, L. Zhou, Magnetic targeted nanoparticles based on β-cyclodextrin and chitosan for hydrophobic drug delivery and a study of their mechanism, RSC Adv. 7 (2017) 29025–29034.
[52] Z. Beji, A. Hanini, L.S. Smiri, J. Gavard, K. Kacem, F. Villain, et al., Magnetic properties of Zn-substituted $MnFe_2O_4$ nanoparticles synthesized in polyol as potential heating agents for hyperthermia. Evaluation of their toxicity on endothelial cells, Chem. Mater. 22 (2010) 5420–5429.
[53] K. Maier-Hauff, F. Ulrich, D. Nestler, H. Niehoff, P. Wust, B. Thiesen, et al., Efficacy and safety of intratumoral thermotherapy using magnetic iron-oxide nanoparticles combined with external beam radiotherapy on patients with recurrent glioblastoma multiforme, J. Neuro Oncol. 103 (2011) 317–324.
[54] M. Johannsen, B. Thiesen, P. Wust, A. Jordan, Magnetic nanoparticle hyperthermia for prostate cancer, Int. J. Hyperth. 26 (2010) 790–795.
[55] A. Bielak-Zmijewska, M. Wnuk, D. Przybylska, W. Grabowska, A. Lewinska, O. Alster, et al., A comparison of replicative senescence and doxorubicin-induced premature senescence of vascular smooth muscle cells isolated from human aorta, Biogerontology 15 (2014) 47–64.
[56] D.R. Green, G. Kroemer, Cytoplasmic functions of the tumour suppressor p53, Nature 458 (2009) 1127–1130.
[57] A. Comel, G. Sorrentino, V. Capaci, G. Del Sal, The cytoplasmic side of p53's oncosuppressive activities, FEBS Lett. 588 (2014) 2600–2609.
[58] J. Cmielova, M. Rezacova, p21Cip1/Waf1 protein and its function based on a subcellular localization [corrected], J. Cell. Biochem. 112 (2011) 3502–3506.
[59] H.V. Hwang, D.T. Tran, M.N. Rebuffatti, C.S. Li, A.A. Knowlton, Investigation of quercetin and hyperoside as senolytics in adult human endothelial cells, PLoS One 13 (2018) e0190374.
[60] L. Geng, Z. Liu, W. Zhang, W. Li, Z. Wu, W. Wang, et al., Chemical screen identifies a geroprotective role of quercetin in premature aging, Protein Cell 10 (2019) 417–435.
[61] A. Salminen, J.M. Hyttinen, K. Kaarniranta, AMP-activated protein kinase inhibits NF-kappaB signaling and inflammation: impact on healthspan and lifespan, J. Mol. Med. (Berl.) 89 (2011) 667–676.
[62] A. Salminen, K. Kaarniranta, AMP-activated protein kinase (AMPK) controls the aging process via an integrated signaling network, Ageing Res. Rev. 11 (2012) 230–241.
[63] Y. Ding, J. Chen, I.S. Okon, M.H. Zou, P. Song, Absence of AMPKalpha2 accelerates cellular senescence via p16 induction in mouse embryonic fibroblasts, Int. J. Biochem. Cell Biol. 71 (2016) 72–80.
[64] J.P. Coppe, C.K. Patil, F. Rodier, Y. Sun, D.P. Munoz, J. Goldstein, et al., Senescence-associated secretory phenotypes reveal cell-nonautonomous functions of oncogenic RAS and the p53 tumor suppressor, PLoS Biol. 6 (2008) 2853–2868.
[65] R.G. Baker, M.S. Hayden, S. Ghosh, NF-kappaB, inflammation, and metabolic disease, Cell Metabol. 13 (2011) 11–22.
[66] S.M. Jeon, Regulation and function of AMPK in physiology and diseases, Exp. Mol. Med. 48 (2016) e245.
[67] J.S. Lee, S.J. Park, Y.S. Cho, J.W. Huh, Y.M. Oh, S.D. Lee, Role of AMP-activated protein kinase (AMPK) in smoking-induced lung inflammation and emphysema, Tuberc. Respir. Dis. 78 (2015) 8–17.
[68] X.Y. Cheng, Y.Y. Li, C. Huang, J. Li, H.W. Yao, AMP-activated protein kinase reduces inflammatory responses and cellular senescence in pulmonary emphysema, Oncotarget 8 (2017) 22513–22523.
[69] L. Galluzzi, F. Pietrocola, B. Levine, G. Kroemer, Metabolic control of autophagy, Cell 159 (2014) 1263–1276.
[70] X. Han, H. Tai, X. Wang, Z. Wang, J. Zhou, X. Wei, et al., AMPK activation protects cells from oxidative stress-induced senescence via autophagic flux restoration and intracellular NAD(+) elevation, Aging Cell 15 (2016) 416–427.
[71] C.D. Wiley, J. Campisi, From ancient pathways to aging cells-connecting metabolism and cellular senescence, Cell Metabol. 23 (2016) 1013–1021.
[72] K.M. Aird, R. Zhang, Metabolic alterations accompanying oncogene-induced senescence, Mol Cell Oncol 1 (2014) e963481.
[73] D.G. Hardie, F.A. Ross, S.A. Hawley, AMPK: a nutrient and energy sensor that maintains energy homeostasis, Nat. Rev. Mol. Cell Biol. 13 (2012) 251–262.
[74] J.S. Kim, E.J. Kim, H.J. Kim, J.Y. Yang, G.S. Hwang, C.W. Kim, Proteomic and metabolomic analysis of H_2O_2-induced premature senescent human mesenchymal stem cells, Exp. Gerontol. 46 (2011) 500–510.
[75] E.L. James, R.D. Michalek, G.N. Pitiyage, A.M. de Castro, K.S. Vignola, J. Jones, et al., Senescent human fibroblasts show increased glycolysis and redox homeostasis with extracellular metabolomes that overlap with those of irreparable DNA damage, aging, and disease, J. Proteome Res. 14 (2015) 1854–1871.
[76] M. Wu, H. Ye, C. Shao, X. Zheng, Q. Li, L. Wang, et al., Metabolomics-proteomics combined approach identifies differential metabolism-associated molecular events between senescence and apoptosis, J. Proteome Res. 16 (2017) 2250–2261.
[77] R.L. Elstrom, D.E. Bauer, M. Buzzai, R. Karnauskas, M.H. Harris, D.R. Plas, et al., Akt stimulates aerobic glycolysis in cancer cells, Cancer Res. 64 (2004) 3892–3899.
[78] R.B. Robey, N. Hay, Is Akt the "Warburg kinase"?-Akt-energy metabolism interactions and oncogenesis, Semin. Cancer Biol. 19 (2009) 25–31.